

The influence of complex thermal treatment on mechanical properties of amorphous materials

Qing-Long Liu¹ and Nikolai V. Priezjev^{1,2}

¹*National Research University Higher School of Economics, Moscow 101000, Russia and*

²*Department of Mechanical and Materials Engineering,*

Wright State University, Dayton, OH 45435

(Dated: March 14, 2022)

Abstract

We study the effect of periodic, spatially uniform temperature variation on mechanical properties and structural relaxation of amorphous alloys using molecular dynamics simulations. The disordered material is modeled via a non-additive binary mixture, which is annealed from the liquid to the glassy state with various cooling rates and then either aged at constant temperature or subjected to thermal treatment. We found that in comparison to aged samples, thermal cycling with respect to a reference temperature of approximately half the glass transition temperature leads to more relaxed states with lower levels of potential energy. The largest energy decrease was observed for rapidly quenched glasses cycled with the thermal amplitude slightly smaller than the reference temperature. Following the thermal treatment, the mechanical properties were probed via uniaxial tensile strain at the reference temperature and constant pressure. The numerical results indicate an inverse correlation between the levels of potential energy and values of the elastic modulus and yield stress as a function of the thermal amplitude.

Keywords: glasses, deformation, temperature, yield stress, molecular dynamics simulations

I. INTRODUCTION

Due to their disordered structure, metallic glasses are known to possess high strength and elastic limit as well as high resistance to corrosion, which makes them potentially suitable for various structural and biomedical applications [1, 2]. These amorphous alloys, however, suffer from lack of ductility and typically exhibit brittle fracture due to shear band formation, especially in aged samples [3]. Commonly used methods to rejuvenate glasses and to improve plasticity, such as shot-peening [4], cold rolling and drawing [5], as well as high-pressure torsion [6], typically cause severe plastic deformation. By contrast, it was recently shown that structural rejuvenation in metallic glasses can be induced by temporarily heating samples above T_g and subsequently quenching with a suitably fast cooling rate for recovery annealing [7, 8]. It was later found that for some alloys, thermal rejuvenation can be enhanced by applying external pressure [9, 10]. Alternatively, rejuvenated states in metallic glasses can be accessed via cryogenic thermal cycling below T_g , which promotes local structural transformations due to spatially non-uniform thermal expansion [11, 12]. The influence of thermal expansion heterogeneity on rejuvenation of metallic glasses was predicted to be important at sufficiently large length scales as compared to scales accessible to atomistic simulations [13]. However, the microscopic details of the thermal processing as well as the degree of rejuvenation or relaxation that can be achieved by applying multiple cycles remain to be clarified.

During the last decade, the dynamic response of amorphous materials to periodic shear deformation was extensively studied using atomistic simulations and experimental measurements [14–28]. Notably, it was shown that thermal aging process in rapidly quenched glasses is facilitated by repetitive subyield cycling that leads to progressively lower levels of potential energy, and the effect is more pronounced at larger strain amplitudes [25, 26, 28]. More recently, it was found that relaxed states can be attained by repeatedly heating and cooling binary glasses at constant pressure with various thermal amplitudes below the glass transition [29, 30]. In particular, the results of numerical simulations have shown that the largest decrease of the potential energy and the increase in the yield stress occur for rapidly cooled glasses with the thermal amplitude not far below the glass transition temperature [29]. It was later found that after hundreds of thermal cycles with respect to a very low reference temperature, the glasses evolve into steady states, where particle dynamics becomes nearly

reversible after each cycle, similar to the so-called limit cycles observed during athermal periodic shear of amorphous materials [17, 19, 30]. However, the dependence of the potential energy and mechanical properties on the preparation history, period and number of thermal oscillations, thermal amplitude, and reference temperature remains unexplored.

In this paper, molecular dynamics simulations are performed to examine the effect of thermal cycling on potential energy states and mechanical properties of binary glasses. The thermal oscillations with relatively small period are imposed with respect to a reference temperature of about half the glass transition temperature. It will be shown that regardless of preparation history, the thermal treatment of one hundred cycles always leads to relaxed states in a wide range of thermal amplitudes. Subsequent tensile loading of aged and thermally cycled glasses reveals that the yield stress and the elastic modulus acquire maxima at the thermal amplitude that corresponds to the most relaxed states.

The paper is structured as follows. The description of molecular dynamics simulations and thermomechanical processing protocols are provided in the next section. The analysis of the potential energy series, particle displacements, and mechanical properties are presented in section III. Brief conclusions are given in the last section.

II. MOLECULAR DYNAMICS SIMULATIONS

The metallic glass is represented by the Kob and Andersen (KA) binary mixture model, which was originally developed to study the amorphous metal alloy $\text{Ni}_{80}\text{P}_{20}$ [31, 32]. In this model, there are two types of atoms, A and B , with strongly non-additive cross interactions that prevent crystallization upon cooling below the glass transition temperature [31]. More specifically, the interaction between two atoms $\alpha, \beta = A, B$ is described by the truncated Lennard-Jones (LJ) potential:

$$V_{\alpha\beta}(r) = 4\varepsilon_{\alpha\beta} \left[\left(\frac{\sigma_{\alpha\beta}}{r} \right)^{12} - \left(\frac{\sigma_{\alpha\beta}}{r} \right)^6 \right], \quad (1)$$

with the following parametrization $\varepsilon_{AA} = 1.0$, $\varepsilon_{AB} = 1.5$, $\varepsilon_{BB} = 0.5$, $\sigma_{AB} = 0.8$, $\sigma_{BB} = 0.88$, and $m_A = m_B$ [31]. The LJ potential is truncated at the cutoff radius $r_{c,\alpha\beta} = 2.5\sigma_{\alpha\beta}$ to alleviate the computational burden. The system is composed of 48000 A atoms and 12000 B atoms, with the total number of atoms of 60000. In what follows, all physical quantities are reported in terms of the reduced LJ units of length, mass, energy, and time: $\sigma = \sigma_{AA}$,

$m = m_A$, $\varepsilon = \varepsilon_{AA}$, and $\tau = \sigma\sqrt{m/\varepsilon}$, respectively. The MD simulations were carried out using the LAMMPS parallel code with the time step $\Delta t_{MD} = 0.005\tau$ [34].

The simulations were performed in several stages. The system was first thoroughly equilibrated at the temperature of $0.7\varepsilon/k_B$, which is above the glass transition of the KA model, $T_g \approx 0.435\varepsilon/k_B$ [31]. Here, k_B denotes the Boltzmann constant. The temperature is controlled via the Nosé-Hoover thermostat, and the periodic boundary conditions are imposed along all three dimensions [33]. After the equilibration procedure, the samples were annealed at constant pressure to the temperature $T_{LJ} = 0.2\varepsilon/k_B$ with the cooling rates $10^{-2}\varepsilon/k_B\tau$, $10^{-3}\varepsilon/k_B\tau$, $10^{-4}\varepsilon/k_B\tau$, and $10^{-5}\varepsilon/k_B\tau$. The snapshot of the binary glass annealed with the cooling rate of $10^{-2}\varepsilon/k_B\tau$ to the temperature of $T_{LJ} = 0.2\varepsilon/k_B$ is illustrated in Fig. 1. Next, the system was repeatedly heated and cooled with the thermal amplitude ΔT_{LJ} during 100 cycles with the period $T = 2000\tau$. The thermal oscillations were imposed at constant pressure, $P = 0$, with respect to the reference temperature $T_{LJ} = 0.2\varepsilon/k_B$. After the thermal treatment, the samples were strained along the \hat{x} direction at constant pressure with the strain rate $\dot{\varepsilon}_{xx} = 10^{-5}\tau^{-1}$. At each stage, the potential energy, pressure components, system dimensions, and atomic configurations were periodically saved for the post-processing analysis.

III. RESULTS

As discussed in Sec. II, the binary mixture was initially equilibrated at the temperature of $0.7\varepsilon/k_B$ and zero pressure, and then annealed below the glass transition point to the temperature of $0.2\varepsilon/k_B$ with different cooling rates. The starting temperature of $0.7\varepsilon/k_B$ was chosen to be not far above the glass transition temperature $T_g \approx 0.435\varepsilon/k_B$ in order to reduce the annealing time during slow cooling and to avoid significant deformation of the simulation domain from a cubic box, since all system dimensions were allowed to vary independently at constant pressure. After the glasses were annealed with the cooling rates $10^{-2}\varepsilon/k_B\tau$, $10^{-3}\varepsilon/k_B\tau$, $10^{-4}\varepsilon/k_B\tau$, and $10^{-5}\varepsilon/k_B\tau$, the simulations proceeded at $T_{LJ} = 0.2\varepsilon/k_B$ and $P = 0$ during the time interval $2 \times 10^5\tau$. The results for the potential energy per atom and the average glass density during the aging process are reported in Fig. 2 for the indicated values of the cooling rate.

It can be observed from Fig. 2 that upon cooling with slower rates, the potential energy

levels become deeper, as the system visits a larger number of minima in the potential energy landscape in the vicinity of the glass transition temperature. During the aging process at $T_{LJ} = 0.2 \varepsilon/k_B$ and $P = 0$, shown in Fig. 2, the potential energy of more rapidly quenched glasses decays significantly during the time interval of $2 \times 10^5 \tau$. A similar decrease of the potential energy during aging below T_g at constant volume during $10^5 \tau$ was reported in the previous MD study, where it was also shown that the system dynamics, as measured by the decay of the two-time intermediate scattering function, becomes progressively slower [35]. We also comment that the potential energy levels reported in the recent study with a similar setup, except that the reference temperature is $T_{LJ} = 0.01 \varepsilon/k_B$, remained nearly constant during the time interval $10^6 \tau$ and relatively low, *i.e.*, $U \lesssim -8.24 \varepsilon$ [29]. As shown in the inset to Fig. 2, the rate of density increase is more pronounced for rapidly cooled glasses, and the difference in the average glass densities after $2 \times 10^5 \tau$ is less than 0.3%.

Following the annealing procedure with different cooling rates, $10^{-2} \varepsilon/k_B \tau$, $10^{-3} \varepsilon/k_B \tau$, $10^{-4} \varepsilon/k_B \tau$, and $10^{-5} \varepsilon/k_B \tau$, the glasses were subjected to repeated cycles of heating and cooling with respect to the reference temperature $T_{LJ} = 0.2 \varepsilon/k_B$. The examples of the selected temperature profiles measured during the first five cycles are presented in Fig. 3 for the glass that was initially annealed with the cooling rate of $10^{-3} \varepsilon/k_B \tau$. In what follows, we denote the maximum deviation from the reference temperature $T_{LJ} = 0.2 \varepsilon/k_B$, or the thermal amplitude, by ΔT_{LJ} . In the present study, we considered a wide range of thermal amplitudes but ensured that temperature remained above zero and below the glass transition temperature. Thus, the maximum value of the thermal amplitude is $\Delta T_{LJ} = 0.19 \varepsilon/k_B$. We also remind that the simulations were carried out at constant pressure ($P = 0$), thus allowing significant variation in volume during each cycle. Here, we emphasize the key differences in the choice of parameters from the previous MD study on thermally cycled binary glasses [29]. Specifically, the thermal treatment was performed with a smaller oscillation period, $T = 2000 \tau$, higher reference temperature, $T_{LJ} = 0.2 \varepsilon/k_B$, and larger number of thermal amplitudes to resolve more accurately the neighborhood around the minimum of the potential energy after 100 cycles (discussed below).

We next present the variation of the potential energy at the beginning and the end of thermal treatment in Figs. 4, 5, 6, and 7 for glasses initially annealed with the cooling

rates $10^{-2}\varepsilon/k_B\tau$, $10^{-3}\varepsilon/k_B\tau$, $10^{-4}\varepsilon/k_B\tau$, and $10^{-5}\varepsilon/k_B\tau$, respectively. For reference, the black curves in each figure denote the data at the constant temperature $T_{LJ} = 0.2\varepsilon/k_B$ (the same data as in Fig. 2). It can be seen that the amplitude of the potential energy oscillations increases at larger thermal amplitudes. From Figs. 4-6, it is apparent that for relatively quickly annealed glasses, the minima of the potential energy become progressively deeper over consecutive cycles for all thermal amplitudes. Moreover, a small difference in the potential energy between aged and thermally cycled glasses is developed after each cycle. This discrepancy becomes especially evident in the enlarged view of the data during the last cycle shown in the insets to Figs. 4-6. By contrast, in the case of slowly annealed glass, shown in Fig. 7, it is difficult to visually detect any changes in the minima of the potential energy from cycle to cycle from the main panels. However, a more detailed view of the data in the inset to Fig. 7 reveals that there is a noticeable deviation in the potential energy after the last cycle for the thermal amplitudes $\Delta T_{LJ} = 0.10\varepsilon/k_B$ and $0.15\varepsilon/k_B$. This implies a nonmonotonic dependence of $U(100T)$ as a function of ΔT_{LJ} .

We next summarize the data for the potential energy after 100 thermal cycles in Fig. 8 as a function of the thermal amplitude for the cooling rates $10^{-2}\varepsilon/k_B\tau$, $10^{-3}\varepsilon/k_B\tau$, $10^{-4}\varepsilon/k_B\tau$, and $10^{-5}\varepsilon/k_B\tau$. The data at $\Delta T_{LJ} = 0$ correspond to the potential energy of glasses aged during the time interval $2 \times 10^5\tau = 100T$ at $T_{LJ} = 0.2\varepsilon/k_B$. The data points in Fig. 8 were obtained by linearly extrapolating the potential energy values in the vicinity of $100T$. It is evident that with increasing thermal amplitude, the potential energy first decreases and then acquires a local minimum at about $\Delta T_{LJ} = 0.17\varepsilon/k_B$. From the data presented in Fig. 8, it is difficult to conclude with certainty whether the minimum in $U(100T)$ versus ΔT_{LJ} depends on the cooling rate. Notice also that the dependence of $U(100T)$ is nearly the same for glasses initially annealed with cooling rates $10^{-2}\varepsilon/k_B\tau$ and $10^{-3}\varepsilon/k_B\tau$.

The increase of the potential energy $U(100T)$ at $\Delta T_{LJ} = 0.18\varepsilon/k_B$ and $0.19\varepsilon/k_B$ in Fig. 8 can be ascribed to relative proximity of the system temperature after a quarter of a cycle, $0.2\varepsilon/k_B + \Delta T_{LJ}$, to the glass transition temperature. In the latter case, the temperature approaches T_g from below, the role of thermal fluctuations temporarily increases, and the systems is then annealed with the effective cooling rate $4\Delta T_{LJ}/T = 0.00038\varepsilon/k_B\tau$ during each cycle. Note that the potential energy of the glass annealed with the cooling rate $10^{-5}\varepsilon/k_B\tau$ and aged at $T_{LJ} = 0.2\varepsilon/k_B$ is nearly the same as $U(100T)$ at $\Delta T_{LJ} = 0.19\varepsilon/k_B$.

A qualitatively similar trend in the dependence of $U(100T)$ on ΔT_{LJ} was reported in the recent study, although the decrease in potential energy due to aging was not so pronounced, since the reference temperature was much lower, *i.e.*, $T_{LJ} = 0.01 \varepsilon/k_B$ [29]. Overall, it can be concluded from Fig. 8 that the sequence of 100 thermal cycles with the reference temperature $T_{LJ} = 0.2 \varepsilon/k_B$ did not grant access to rejuvenated states and resulted only in relaxed states for all cooling rates and thermal amplitudes considered in the present study.

The analysis of atomic displacements during consecutive cycles revealed that the relaxation process proceeds via irreversible rearrangements of groups of atoms. We first examine the distribution of displacements during selected cycles for thermal cycling with the amplitude $\Delta T_{LJ} = 0.10 \varepsilon/k_B$. The results are presented in Fig. 9 for binary glasses annealed with cooling rates $10^{-2} \varepsilon/k_B \tau$ and $10^{-5} \varepsilon/k_B \tau$. It can be observed from Fig. 9 (a) that in the rapidly cooled glass, the distribution of displacements is relatively broad during the first few cycles, implying that a large number of atoms with displacements much greater than the cage size, $r_c \approx 0.1 \sigma$, undergo irreversible rearrangements, or cage jumps, after one cycle. However, after 100 thermal cycles, the distribution function becomes more narrow, indicating progressively more reversible particle dynamics. By contrast, as evident from Fig. 9 (b), the shape of the distribution of displacements for slowly annealed glass is rather insensitive to the cycle number, and only a relatively small number of atoms might change their cages during one cycle.

We next discuss the distribution of atomic displacements at the beginning of the thermal treatment, *i.e.*, during the second cycle, but consider instead the effect of the thermal amplitude. The probability distributions are plotted in Fig. 10 for selected values of the thermal amplitude and cooling rates $10^{-2} \varepsilon/k_B \tau$ and $10^{-5} \varepsilon/k_B \tau$. As shown in Fig. 10 (a), the distribution of displacements is much broader at the thermal amplitude $\Delta T_{LJ} = 0.19 \varepsilon/k_B$, and it narrows upon decreasing ΔT_{LJ} towards the limiting case of aging at constant temperature. A similar trend can be observed for the slowly cooled glass in Fig. 10 (b) but the effect is less pronounced. In general, these results are consistent with the analysis of nonaffine displacements during thermal cycling with respect to a very low reference temperature reported in the previous study [29]. In particular, it was shown that atoms with large nonaffine displacements after one cycle are organized into transient clusters, whose size is reduced with increasing cycle number or decreasing cooling rate and thermal amplitude [29].

After the thermal treatment, the samples were strained along the \hat{x} direction with constant strain rate $\dot{\varepsilon}_{xx} = 10^{-5} \tau^{-1}$ at $T_{LJ} = 0.2 \varepsilon/k_B$ and zero pressure. The resulting stress-strain response for different cooling rates is presented in Fig. 11. For reference, the data for tensile stress as a function of strain for glasses aged at $T_{LJ} = 0.2 \varepsilon/k_B$ during $2 \times 10^5 \tau$ are also included in Fig. 11 and indicated by black curves. All samples were strained up to $\varepsilon_{xx} = 0.25$ until the tensile stress is saturated to a constant value independent of the processing history. Following the elastic regime of deformation, the stress-strain curves exhibit a pronounced yielding peak at about $\varepsilon_{xx} = 0.05$. It can be observed in each panel in Fig. 11 that the magnitude of the peak becomes larger with increasing thermal amplitude up to $\Delta T_{LJ} \approx 0.15 \varepsilon/k_B$. Notice, however, that the stress overshoot is generally reduced from the maximum value when $\Delta T_{LJ} = 0.19 \varepsilon/k_B$ for all cooling rates. These results indicate a nonmonotonic variation of the yield stress on the thermal amplitude.

The stress-strain curves reported in Fig. 11 were used to extract the values of the yielding peak, σ_Y , and the elastic modulus, E , which are plotted in Fig. 12 as a function of the thermal amplitude. It can be seen that σ_Y increases with ΔT_{LJ} and it has a maximum at $\Delta T_{LJ} \approx 0.15 \varepsilon/k_B$ for all cooling rates. Note that the data are somewhat scattered as simulations were performed for only one sample in each case due to computational limitations. We also comment that the yield stress only weakly depends on the cooling rate except for the case $10^{-5} \varepsilon/k_B \tau$. Similar trends can be observed for the dependence of the elastic modulus on the thermal amplitude and cooling rate, as illustrated in the inset to Fig. 12. Generally, we find an inverse correlation between the dependencies of the yielding peak in Fig. 12 and $U(100T)$ in Fig. 8 as functions of the thermal amplitude ΔT_{LJ} . In other words, the lower the energy state, the higher the values of σ_Y and E . Finally, in comparison with the results of the previous study, where thermal cycling was performed with respect to a much lower reference temperature of $0.01 \varepsilon/k_B$ [29], the relative increase in σ_Y and, correspondingly, decrease in $U(100T)$ for rapidly cooled glasses is less pronounced for cycling with respect to the reference temperature of $0.2 \varepsilon/k_B$, considered in the present study.

IV. CONCLUSIONS

In summary, the response of amorphous alloys during the sequence of quenching, periodic thermal treatment, and tensile loading was investigated using molecular dynamics

simulations. The amorphous material was represented via a binary mixture of atoms with highly non-additive cross interactions that prevents crystallization upon cooling. The thermal quenching was performed at constant pressure by cooling the binary mixture from the liquid state into the glassy region with different rates. The reference temperature was chosen to be approximately half the glass transition temperature, and the simulations were performed at zero pressure.

After the thermal quench to different energy states, the glasses were either set to age at the reference temperature or subjected to one hundred thermal cycles of spatially uniform heating and cooling at constant pressure. It was found that thermal cycling leads to relaxed states with the potential energy levels lower than those in the aged samples for a given value of the cooling rate. The potential energy after one hundred cycles acquired a minimum at the thermal amplitude just below the reference temperature. The results of uniaxial tensile loading demonstrated that the stress overshoot and the elastic modulus only weakly depend on the cooling rate except for the lowest rate. Overall, the inverse correlation between the potential energy levels and mechanical properties for different thermal amplitudes agrees well with the results of the previous study [29], although the magnitude of the effects are slightly reduced due to the higher reference temperature considered in the present study.

Acknowledgments

Financial support from the National Science Foundation (CNS-1531923) is gratefully acknowledged. The article was prepared within the framework of the Basic Research Program at the National Research University Higher School of Economics (HSE) and supported within the framework of a subsidy by the Russian Academic Excellence Project ‘5-100’. The molecular dynamics simulations were performed using the LAMMPS numerical code developed at Sandia National Laboratories [34]. Computational work in support of this research was performed at Wright State University’s Computing Facility, the Ohio Supercomputer Center, and the HPC cluster at Skoltech.

[1] T. Egami, T. Iwashita, and W. Dmowski, Mechanical properties of metallic glasses, *Metals* **3**, 77 (2013).

- [2] H. F. Li and Y. F. Zheng, Recent advances in bulk metallic glasses for biomedical applications, *Acta Biomaterialia* **36**, 1 (2016).
- [3] X. K. Xi, D. Q. Zhao, M. X. Pan, W. H. Wang, Y. Wu, and J. J. Lewandowski, Fracture of brittle metallic glasses: Brittleness or plasticity, *Phys. Rev. Lett.* **94**, 125510 (2005).
- [4] A. Concustell, F. O. Mear, S. Surinach, M. D. Baro and A. L. Greer, Structural relaxation and rejuvenation in a metallic glass induced by shot-peening, *Philos. Mag. Lett.* **89**, 831 (2009).
- [5] K. K. Song, S. Pauly, Y. Zhang, S. Scudino, P. Gargarella, K. B. Surreddi, U. Kuhn, and J. Eckert, Significant tensile ductility induced by cold rolling in $\text{Cu}_{47.5}\text{Zr}_{47.5}\text{Al}_5$ bulk metallic glass, *Intermetallics* **19**, 1394 (2011).
- [6] S.-H. Joo, D.-H. Pi, A. D. H. Setyawan, H. Kato, M. Janecek, Y. C. Kim, S. Lee, and H. S. Kim, Work-hardening induced tensile ductility of bulk metallic glasses via high-pressure torsion, *Sci. Rep.* **5**, 9660 (2015).
- [7] M. Wakeda, J. Saida, J. Li, and S. Ogata, Controlled rejuvenation of amorphous metals with thermal processing, *Sci. Rep.* **5**, 10545 (2015).
- [8] J. Saida, R. Yamada, M. Wakeda, and S. Ogata, Thermal rejuvenation in metallic glasses, *Sci. Technol. Adv. Mater.* **18**, 152 (2017).
- [9] N. Miyazaki, M. Wakeda, Y.-J. Wang, and S. Ogata, Prediction of pressure-promoted thermal rejuvenation in metallic glasses, *NPJ Comput. Mater.* **2**, 16013 (2016).
- [10] M. Wang, H. Liu, J. Mo, Y. Zhang, Z. Chen, C. Yin, and W. Yang, Thermal-pressure effects on energy state of metallic glass $\text{Cu}_{50}\text{Zr}_{50}$, *Comput. Mater. Sci.* **155**, 493 (2018).
- [11] S. V. Ketov, Y. H. Sun, S. Nachum, Z. Lu, A. Checchi, A. R. Beraldin, H. Y. Bai, W. H. Wang, D. V. Louzguine-Luzgin, M. A. Carpenter, and A. L. Greer, Rejuvenation of metallic glasses by non-affine thermal strain, *Nature* **524**, 200 (2015).
- [12] T. J. Lei, L. R. DaCosta, M. Liu, W. H. Wang, Y. H. Sun, A. L. Greer, and M. Atzmon, Microscopic characterization of structural relaxation and cryogenic rejuvenation in metallic glasses, *Acta Mater.* **164**, 165 (2019).
- [13] B. Shang, P. Guan, and J.-L. Barrat, Role of thermal expansion heterogeneity in the cryogenic rejuvenation of metallic glasses, *J. Phys.: Mater.* **1**, 015001 (2018).
- [14] D. J. Lacks and M. J. Osborne, Energy landscape picture of overaging and rejuvenation in a sheared glass, *Phys. Rev. Lett.* **93**, 255501 (2004).
- [15] N. V. Priezjev, Heterogeneous relaxation dynamics in amorphous materials under cyclic load-

- ing, Phys. Rev. E **87**, 052302 (2013).
- [16] D. Fiocco, G. Foffi, and S. Sastry, Oscillatory athermal quasistatic deformation of a model glass, Phys. Rev. E **88**, 020301(R) (2013).
 - [17] I. Regev, T. Lookman, and C. Reichhardt, Onset of irreversibility and chaos in amorphous solids under periodic shear, Phys. Rev. E **88**, 062401 (2013).
 - [18] N. V. Priezjev, Dynamical heterogeneity in periodically deformed polymer glasses, Phys. Rev. E **89**, 012601 (2014).
 - [19] I. Regev, J. Weber, C. Reichhardt, K. A. Dahmen, and T. Lookman, Reversibility and criticality in amorphous solids, Nat. Commun. **6**, 8805 (2015).
 - [20] N. V. Priezjev, Reversible plastic events during oscillatory deformation of amorphous solids, Phys. Rev. E **93**, 013001 (2016).
 - [21] N. V. Priezjev, Nonaffine rearrangements of atoms in deformed and quiescent binary glasses, Phys. Rev. E **94**, 023004 (2016).
 - [22] P. Leishangthem, A. D. S. Parmar, and S. Sastry, The yielding transition in amorphous solids under oscillatory shear deformation, Nat. Commun. **8**, 14653 (2017).
 - [23] N. V. Priezjev, Collective nonaffine displacements in amorphous materials during large-amplitude oscillatory shear, Phys. Rev. E **95**, 023002 (2017).
 - [24] I. Buttinoni, M. Steinacher, H. Th. Spanke, J. Pokki, S. Bahmann, B. Nelson, G. Foffi, and L. Isa, Colloidal polycrystalline monolayers under oscillatory shear, Phys. Rev. E **95**, 012610 (2017).
 - [25] N. V. Priezjev, Molecular dynamics simulations of the mechanical annealing process in metallic glasses: Effects of strain amplitude and temperature, J. Non-Cryst. Solids **479**, 42 (2018).
 - [26] N. V. Priezjev, The yielding transition in periodically sheared binary glasses at finite temperature, Comput. Mater. Sci. **150**, 162 (2018).
 - [27] M. C. Rogers, K. Chen, M. J. Pagenkopp, T. G. Mason, S. Narayanan, J. L. Harden, and R. L. Leheny, Microscopic signatures of yielding in concentrated nanoemulsions under large-amplitude oscillatory shear, Phys. Rev. Materials **2**, 095601 (2018).
 - [28] N. V. Priezjev, Slow relaxation dynamics in binary glasses during stress-controlled, tension-compression cyclic loading, Comput. Mater. Sci. **153**, 235 (2018).
 - [29] N. V. Priezjev, The effect of cryogenic thermal cycling on aging, rejuvenation, and mechanical properties of metallic glasses, J. Non-Cryst. Solids **502** (2018).

<https://doi.org/10.1016/j.jnoncrysol.2018.09.041>

- [30] N. V. Priezjev, The potential energy states and mechanical properties of thermally cycled binary glasses, arXiv:1810.10877 (2018).
- [31] W. Kob and H. C. Andersen, Testing mode-coupling theory for a supercooled binary Lennard-Jones mixture: The van Hove correlation function, Phys. Rev. E **51**, 4626 (1995).
- [32] T. A. Weber and F. H. Stillinger, Local order and structural transitions in amorphous metal-metalloid alloys, Phys. Rev. B **31**, 1954 (1985).
- [33] M. P. Allen and D. J. Tildesley, *Computer Simulation of Liquids* (Clarendon, Oxford, 1987).
- [34] S. J. Plimpton, Fast parallel algorithms for short-range molecular dynamics, J. Comp. Phys. **117**, 1 (1995).
- [35] W. Kob and J.-L. Barrat, Aging effects in a Lennard-Jones glass, Phys. Rev. Lett. **78**, 4581 (1997).

Figures

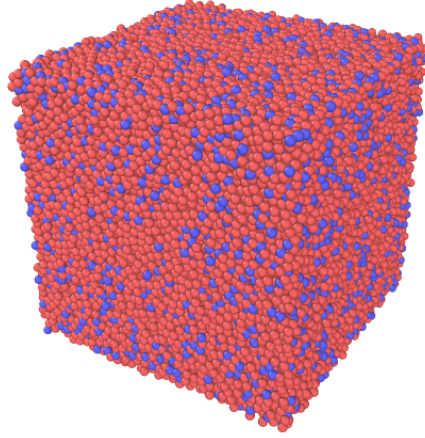


FIG. 1: (Color online) A representative snapshot of the binary LJ glass annealed with the cooling rate of $10^{-2}\varepsilon/k_B\tau$ to the temperature $T_{LJ} = 0.2\varepsilon/k_B$. The total number of atoms is 60 000. The larger atoms of type A are denoted by red spheres and smaller atoms of type B are indicated by blue spheres.

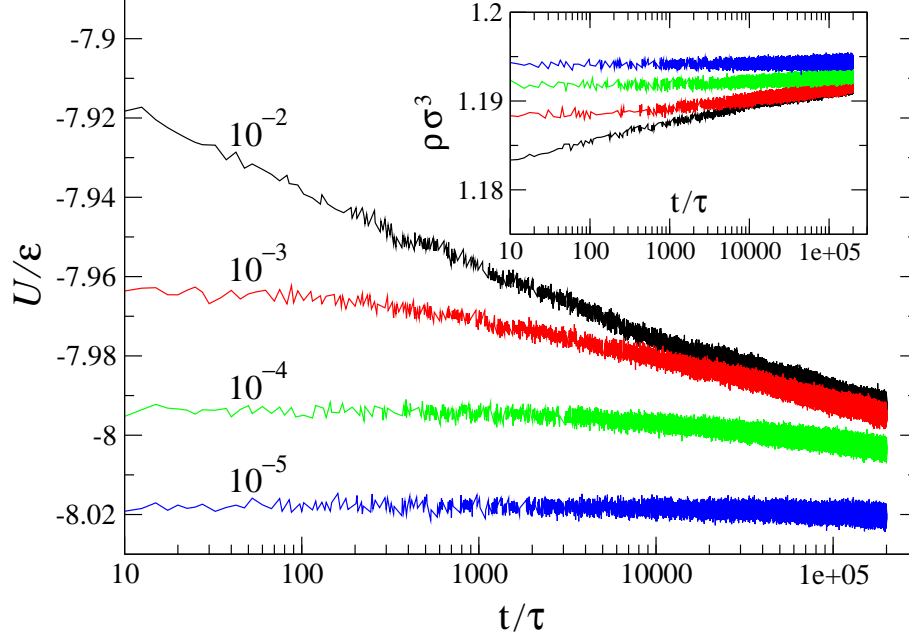


FIG. 2: (Color online) The variation of the potential energy per atom for binary glasses prepared with cooling rates $10^{-2}\varepsilon/k_B\tau$ (black), $10^{-3}\varepsilon/k_B\tau$ (red), $10^{-4}\varepsilon/k_B\tau$ (green), and $10^{-5}\varepsilon/k_B\tau$ (blue). The simulations are performed at constant temperature $T_{LJ} = 0.2\varepsilon/k_B$ and zero pressure. The inset shows the glass density as a function of time for the same samples.

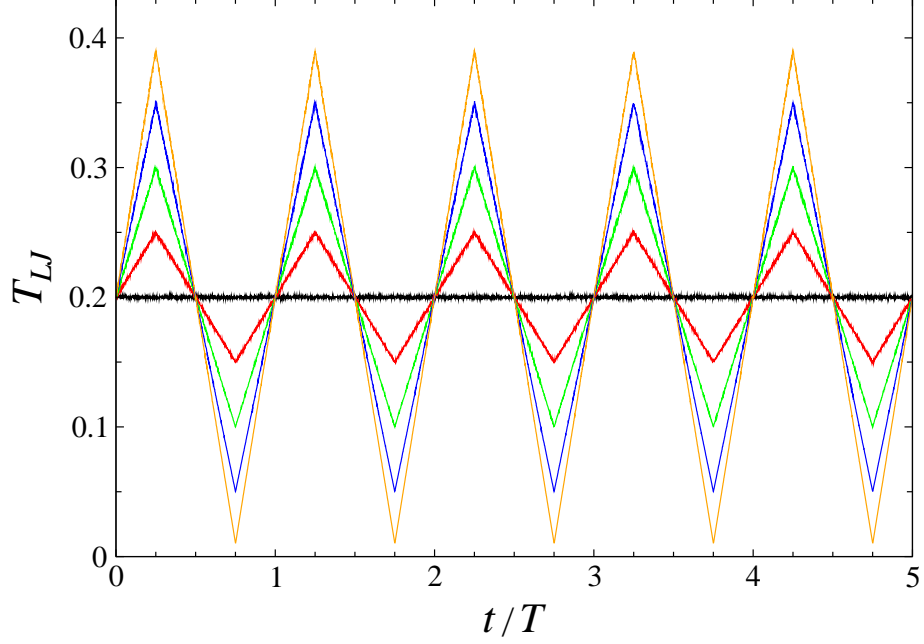


FIG. 3: (Color online) The variation of temperature T_{LJ} (in units of ε/k_B) during 5 periods, $T = 2000\tau$, for the thermal amplitudes $\Delta T_{LJ} = 0.05\varepsilon/k_B$ (red), $0.10\varepsilon/k_B$ (green), $0.15\varepsilon/k_B$ (blue), and $0.19\varepsilon/k_B$ (orange). The black line denotes the data at the constant temperature $T_{LJ} = 0.2\varepsilon/k_B$. The data are taken in the binary glass initially annealed with the cooling rate of $10^{-3}\varepsilon/k_B\tau$ to the temperature $T_{LJ} = 0.2\varepsilon/k_B$.

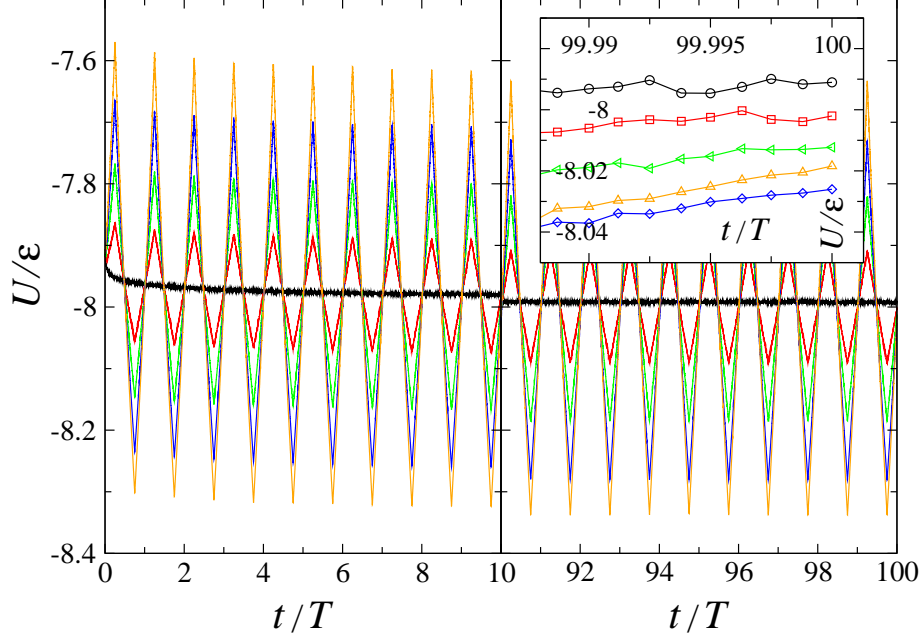


FIG. 4: (Color online) The potential energy series during the first and last ten cycles with the thermal amplitudes $\Delta T_{LJ} = 0$ (black), $0.05\epsilon/k_B$ (red), $0.1\epsilon/k_B$ (green), $0.15\epsilon/k_B$ (blue), and $0.19\epsilon/k_B$ (orange). The sample was initially annealed with the cooling rate of $10^{-2}\epsilon/k_B\tau$. The enlarged view of the same data at the end of the last cycle is displayed in the inset.

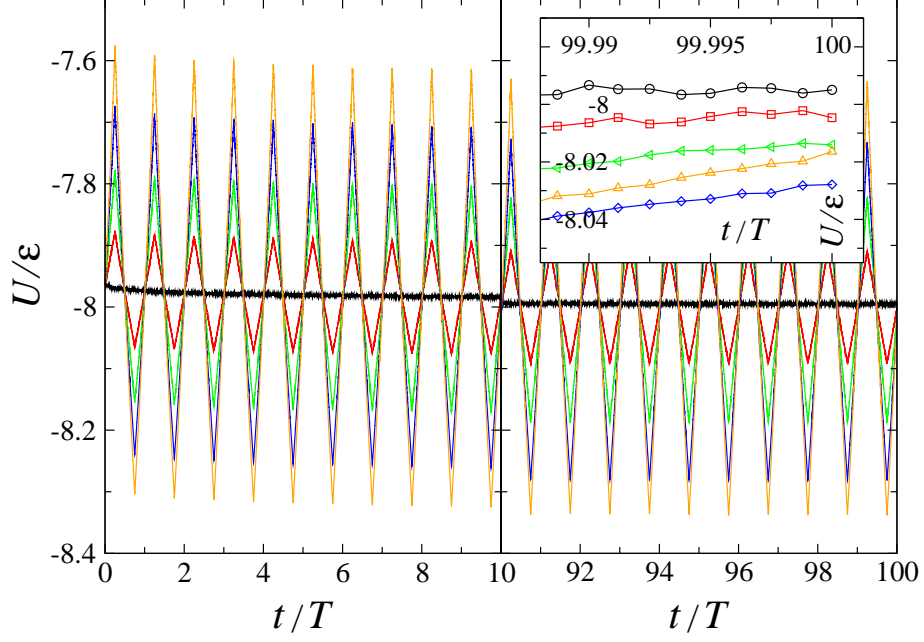


FIG. 5: (Color online) The variation of the potential energy for the glass annealed with the cooling rate of $10^{-3} \varepsilon/k_B \tau$ and subjected to thermal cycling with the amplitudes $\Delta T_{LJ} = 0$ (black), $0.05 \varepsilon/k_B$ (red), $0.1 \varepsilon/k_B$ (green), $0.15 \varepsilon/k_B$ (blue), and $0.19 \varepsilon/k_B$ (orange). The inset shows U at $t \approx 100 T$.

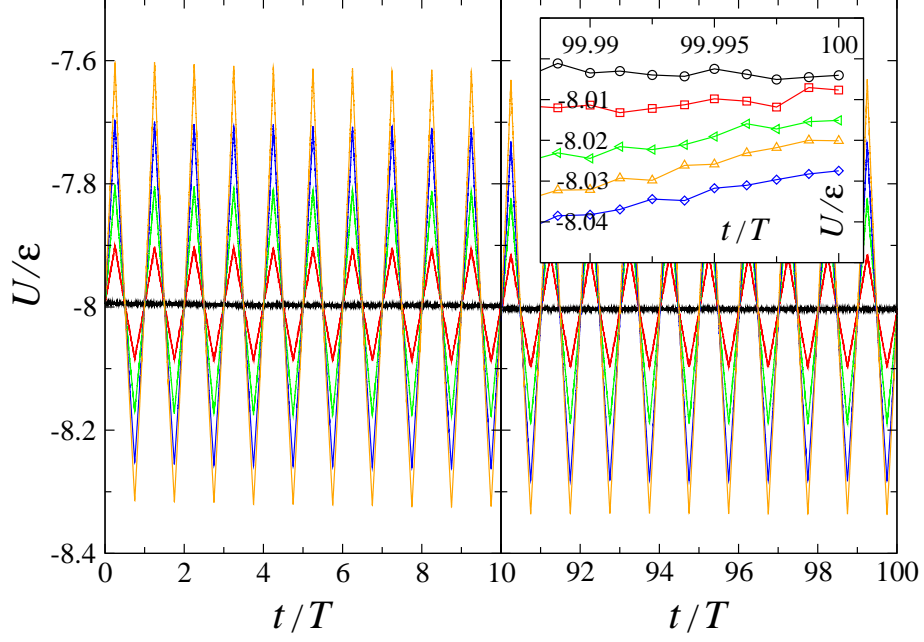


FIG. 6: (Color online) The potential energy per atom, U/ε , for glasses cycled with the amplitudes $\Delta T_{LJ} = 0$ (black), $0.05 \varepsilon/k_B$ (red), $0.1 \varepsilon/k_B$ (green), $0.15 \varepsilon/k_B$ (blue), and $0.19 \varepsilon/k_B$ (orange). The cooling rate is $10^{-4} \varepsilon/k_B \tau$. The same data are resolved near $t \approx 100 T$ and shown in the inset.

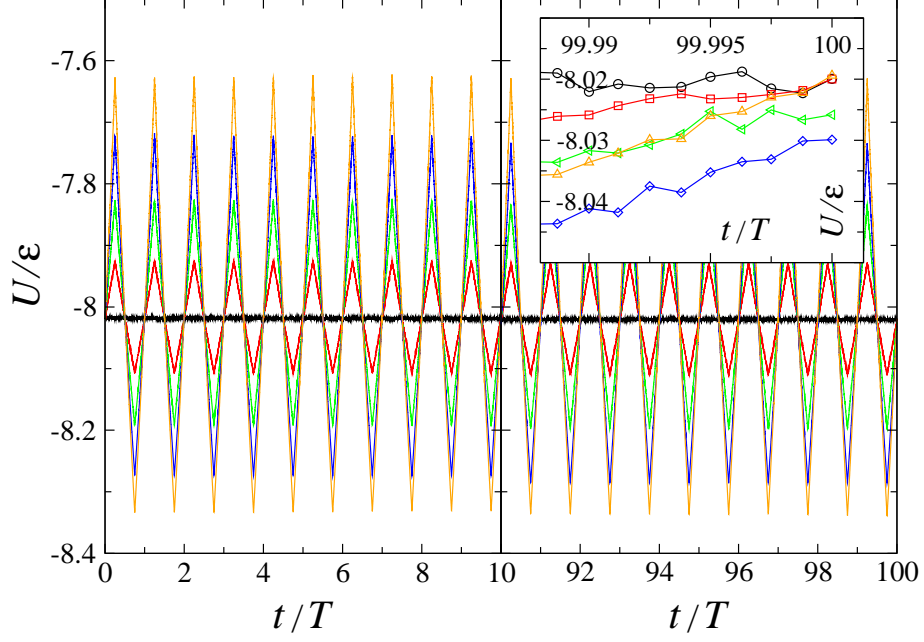


FIG. 7: (Color online) The time dependence of the potential energy during thermal treatment with amplitudes $\Delta T_{LJ} = 0$ (black), $0.05 \varepsilon/k_B$ (red), $0.1 \varepsilon/k_B$ (green), $0.15 \varepsilon/k_B$ (blue), and $0.19 \varepsilon/k_B$ (orange). The sample was initially cooled with the rate $10^{-5} \varepsilon/k_B \tau$. The inset shows the same data in the vicinity of $t \approx 100 T$.

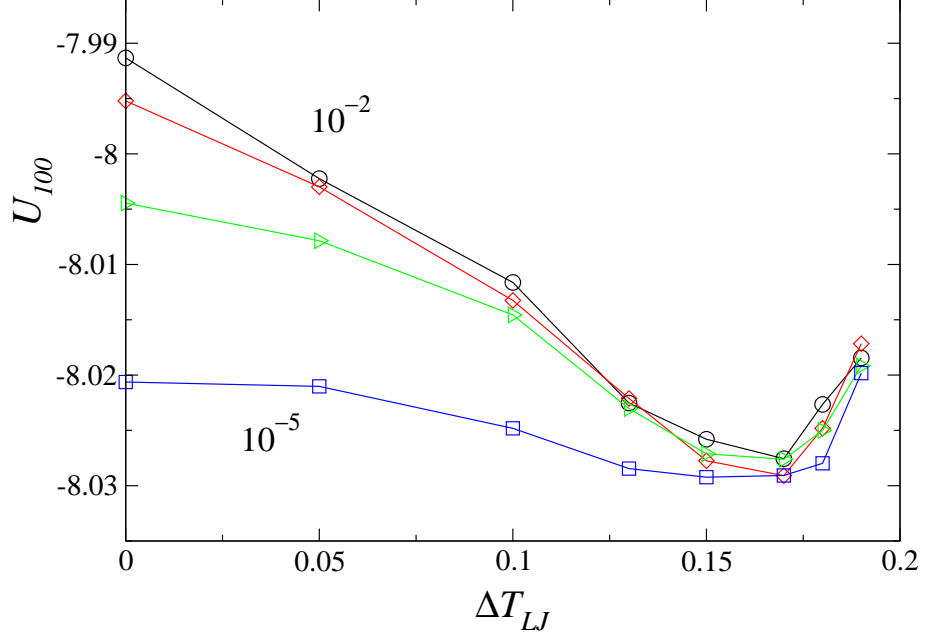


FIG. 8: (Color online) The dependence of the potential energy after 100 cycles, U_{100}/ε , as a function of the thermal amplitude ΔT_{LJ} (in units of ε/k_B) for glasses initially annealed with the cooling rates of $10^{-2}\varepsilon/k_B\tau$ (black), $10^{-3}\varepsilon/k_B\tau$ (red), $10^{-4}\varepsilon/k_B\tau$ (green), and $10^{-5}\varepsilon/k_B\tau$ (blue).

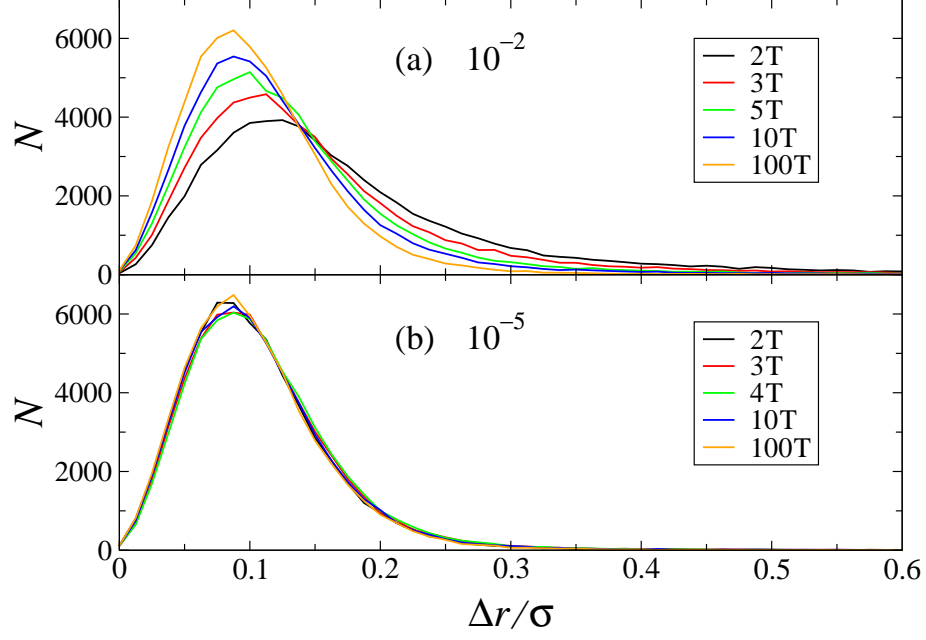


FIG. 9: (Color online) The distribution of atomic displacements during one cycle for the thermal amplitude $\Delta T_{LJ} = 0.10 \epsilon/k_B$. The cycle numbers for computing the displacements are tabulated in the legend. The data are reported for glasses initially annealed with cooling rates (a) $10^{-2} \epsilon/k_B \tau$ and (b) $10^{-5} \epsilon/k_B \tau$. The period of thermal oscillations is $T = 2000 \tau$.

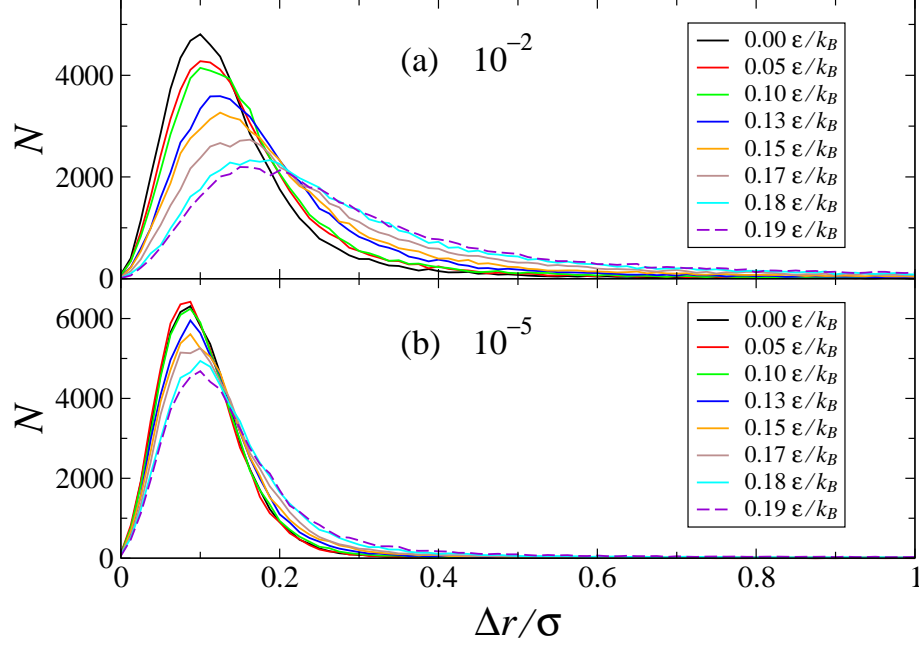


FIG. 10: (Color online) The probability distribution of atomic displacements during the second cycle for the indicated values of the thermal amplitude ΔT_{LJ} . The samples were initially prepared with cooling rates (a) $10^{-2}\varepsilon/k_B\tau$ and (b) $10^{-5}\varepsilon/k_B\tau$.

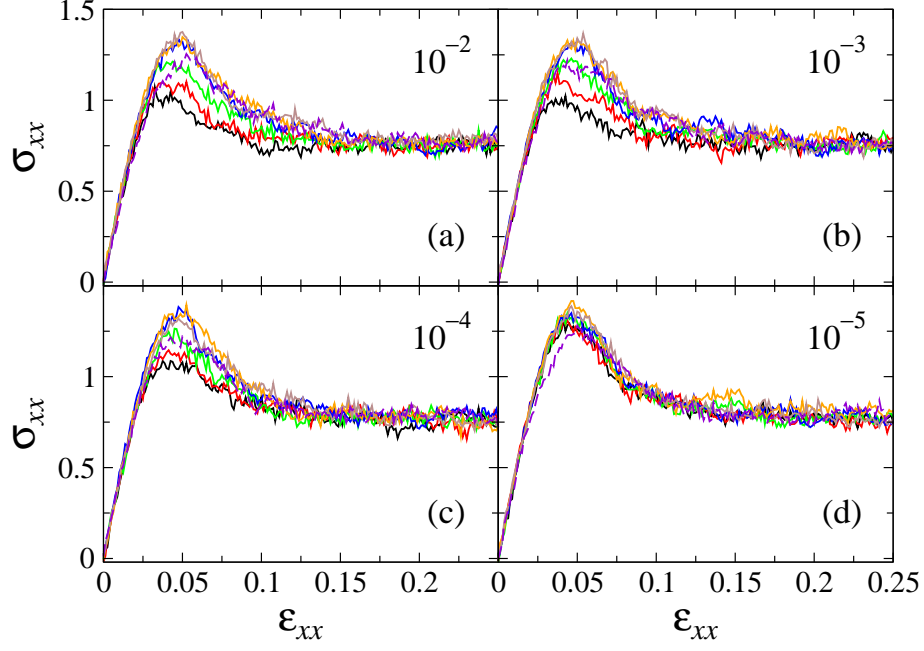


FIG. 11: (Color online) The variation of tensile stress, σ_{xx} (in units of $\varepsilon\sigma^{-3}$), as a function of strain, ε_{xx} , for thermally treated glasses that were initially annealed with cooling rates (a) $10^{-2}\varepsilon/k_B\tau$, (b) $10^{-3}\varepsilon/k_B\tau$, (c) $10^{-4}\varepsilon/k_B\tau$, and (d) $10^{-5}\varepsilon/k_B\tau$. The strain rate is $\dot{\varepsilon}_{xx} = 10^{-5}\tau^{-1}$. The tensile tests were performed after the thermal treatment with amplitudes $\Delta T_{LJ} = 0$ (black), $0.05\varepsilon/k_B$ (red), $0.10\varepsilon/k_B$ (green), $0.13\varepsilon/k_B$ (blue), $0.15\varepsilon/k_B$ (orange), $0.17\varepsilon/k_B$ (brown), and $0.19\varepsilon/k_B$ (dashed violet).

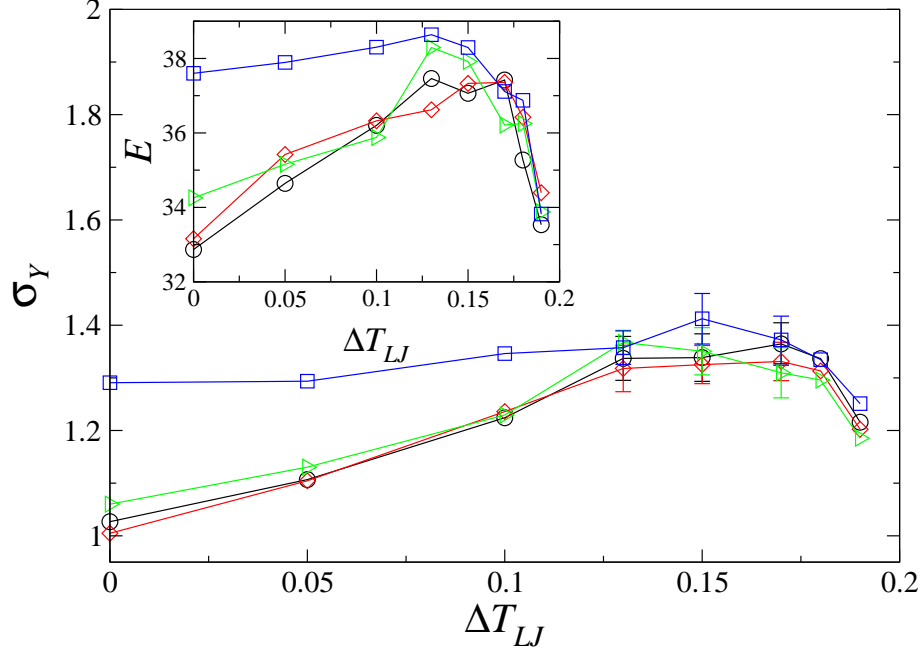


FIG. 12: (Color online) The dependence of the stress overshoot σ_Y (in units of $\varepsilon\sigma^{-3}$) as a function of the thermal amplitude for glasses annealed with cooling rates $10^{-2}\varepsilon/k_B\tau$ (black), $10^{-3}\varepsilon/k_B\tau$ (red), $10^{-4}\varepsilon/k_B\tau$ (green), and $10^{-5}\varepsilon/k_B\tau$ (blue). The variation of the elastic modulus E (in units of $\varepsilon\sigma^{-3}$) versus thermal amplitude is shown in the inset for the same samples.